Imaging of zinc oxide nanoparticle penetration in human skin *in vitro* and *in vivo*

Andrei V. Zvyagin
Xin Zhao
Macquarie University
Department of Physics
Centre of MQ Photonics
Sydney, NSW 2109, Australia

Audrey Gierden
Université Claude Bernard Lyon
Institut des Sciences Pharmaceutiques et Biologiques
Lyon, France

Washington Sanchez
Justin A. Ross
Michael S. Roberts
The University of Queensland
School of Medicine
Therapeutics Research Unit
Princess Alexandra Hospital
Australia

Abstract. Zinc oxide (ZnO-nano) and titanium dioxide nanoparticles (20 to 30 nm) are widely used in several topical skin care products, such as sunscreens. However, relatively few studies have addressed the subdermal absorption of these nanoparticles *in vivo*. We report on investigation of the distribution of topically applied ZnO in excised and *in vivo* human skin, using multiphoton microscopy (MPM) imaging with a combination of scanning electron microscopy (SEM) and an energy-dispersive x-ray (EDX) technique to determine the level of penetration of nanoparticles into the sub-dermal layers of the skin. The good visualization of ZnO in skin achieved appeared to result from two factors. First, the ZnO principal photoluminescence at 385 nm is in the "quiet" spectral band of skin autofluorescence dominated by the endogenous skin fluorophores, i.e., NAD[P]H and FAD. Second, the two-photon action cross section of ZnO-nano [$\sigma_{ZnO}^{(TPEF)}$ ~ 0.26 GM; diameter, 18 nm] is high: $\sim$500-fold of that inferred from its bulk third-order nonlinear susceptibility [Im $\chi_{ZnO}^{(3)}$], and is favorably compared to that of NAD[P]H and FAD. The overall outcome from MPM, SEM, and EDX studies was that, in humans *in vivo*, ZnO nanoparticles stayed in the stratum corneum (SC) and accumulated into skin folds and/or hair follicle roots of human skin. Given the lack of penetration of these nanoparticles past the SC and that the outermost layers of SC have a good turnover rate, these data suggest that the form of ZnO-nano studied here is unlikely to result in safety concerns. © *2008 Society of Photo-Optical Instrumentation Engineers.*
[DOI: 10.1117/1.3041492]

Keywords: nonlinear optical microscopy; nanoparticle toxicity; zinc oxide; transdermal permeability; multiphoton microscopy.

Paper 08185R received Jun. 13, 2008; revised manuscript received Sep. 5, 2008; accepted for publication Oct. 20, 2008; published online Dec. 23, 2008.

1 Introduction

Nanomaterials including nanoemulsions, nanosomes, and nanoparticles are employed as active components[1,2] and delivery vehicles[3,4] in cosmetics and medicine. One example of a nanotechnology application is the widespread use of zinc oxide (ZnO-nano) and titanium dioxide (TiO$_2$) nanoparticles as ingredients in cosmetic and sun-blocking creams. These nanomaterials are efficient absorbers of the ultraviolet (UV) radiation: ZnO absorbs both UVA (400 to 320 nm) and UVB (320 to 290 nm) radiation and reemits them as less damaging UVA or as visible fluorescence (and is dictated by the need to minimize skin damage due to UV light and potential consequences such as skin cancer). The use of these sun-blocking creams is widespread in Australia, where over 250,000 people are diagnosed with nonmelanoma skin cancer, and over 8000 with melanoma annually.[5]

The upper size limit for ZnO and TiO$_2$ nanoparticles is dictated by the aesthetic marketing value of transparent sun-blocking creams. Transparency is achieved by reducing scattering efficiency of ZnO particles, which are normally white and visible, by using a nanoparticle size of less than 30 nm, its transparency threshold.[6] An inevitable question then is whether there a potential toxicity of these nanoparticles whose size may be small enough to allow them to penetrate the skin. The extent of nanoparticles penetration through the topmost layer of the skin, stratum corneum (average thickness, less than 20 μm) into the viable epidermis, is hotly debated. As an illustration, the studies of Alvarez-Roman et al. shows no penetration through excised human skin.[6] In contrast, Ryman-Rasmussen[33] show extensive penetration of neutral, positively charged and negatively charged quantum dots through pig skin. *In vitro* cytotoxicity of ZnO-nano to epidermal (and, especially, epithelial) cells can occur and have been attributed to free radical generation (mainly via hydroxyl radicals formed through oxidation), causing adverse effects in isolated cell experiments.[8,9]

Conventional scanning electron microscopy (SEM), transmission electron microscopy and Franz cell penetration in-

Address all correspondence to: Andrei V. Zvyagin, Dept. of Physics, Centre of MQ Photonics, Macquarie Univ., Sydney, NSW 2109, Australia; Tel: +61 2 9850 7760; Fax: +61 2 9850 7760 8115; Email: azvyagin@ics.mq.edu.au

volve indirect or/and destructive sampling of skin that limits the experimental methods to *in vitro* observations. Optical microscopy of nanoparticle distribution in skin *in vivo* is precluded due to high scattering efficiency of the superficial layers of skin, especially human skin. Fluorescence confocal microscopy has enabled production of clear subsurface images of skin at depths down to ~100 μm at the micrometer resolution by way of "optical sectioning" thin layers of the specimen. The skin morphology contrast is derived from the skin autofluorescence, although often requires additional staining. The visibility of nanoparticles depends on their fluorescent properties, which limits the choice to the following materials: micro- and nanobeads impregnated with fluorescence dye molecules, photoluminescent nanomaterials, quantum dot (Qdot) structures,[10] and emerging nanocrystals with color centers.[11] Fabrication of nanobeads impregnated with fluorescent dye is difficult and they are prone to photobleaching. Qdots are cytotoxic, thus, posing hazard for *in vivo* applications on humans. Although silica Qdots are less cytotoxic, their photoluminescence (PL) degradation and complex passivation chemistry makes their application cumbersome and expensive.[12] PL materials, such as semiconductor metal oxides, are either toxic, radiation-inefficient (due to the indirect band gap structure), or rare. In contrast, ZnO-nano represents a promising nanomaterial that is widespread, inexpensive, and has proven to be suitable for cosmetic care and pharmacy. Its production is straightforward, yielding nanoparticle of various sizes and shapes, starting from 3 nm and larger.[7,13] ZnO material properties, including a direct wide bandgap (3.4 eV) electronic structure, and high exciton energy of 60 meV (compare to that of 25 meV of cadmium selenide), are very attractive for a new generation of electrooptic devices, e.g., light-emitting diodes and lasers in the UV spectral range. The wide bandgap of ZnO requires excitation at a wavelength of 320 nm in the UV spectral range, with principle emission at 385 nm, as shown in Fig. 1 (scattered squares graph). This excitation requirement is problematic for application of ZnO-nano in optical biomedical imaging. First, UV photons efficiently excite a number of intrinsic (endogenous) fluorophores in skin that produce a broadband autofluorescence background. Among these, nicotinamide adenine dinucleotide/nicotinamide adenine dinucleotide phosphate (NAD[P]H), flavin adenine dinucleotide (FAD), and porphyrins contribute 75, 25, and 2% to the skin autofluorescence, with their respective fluorescence bands centered at 425, 520, and 625 nm (Ref. 15) [also see Fig. 1(a)]. Second, UV radiation is heavily absorbed and scattered by the skin tissue, severely limiting imaging penetration depth. Hence, optical imaging of thick skin tissue using UV light is not practical.

It has been recently found that the zinc oxide structure is efficiently excited via a nonlinear optical process of simultaneous absorption of two or three photons under illumination by an ultrashort-pulse laser.[16] This shifts the ZnO excitation band to the infrared (IR) range, where the ultrashort-pulse laser sources predominantly operate, falling into the so-called therapeutic window, 600 to 1400 nm, wherein the maximum imaging penetration depth in tissue of ~200 μm is attainable. The increased penetration depth is due, first, to the markedly reduced absorption of the major tissue constituents, including proteins, hemoglobin, and melanin in the UV/visible spectral
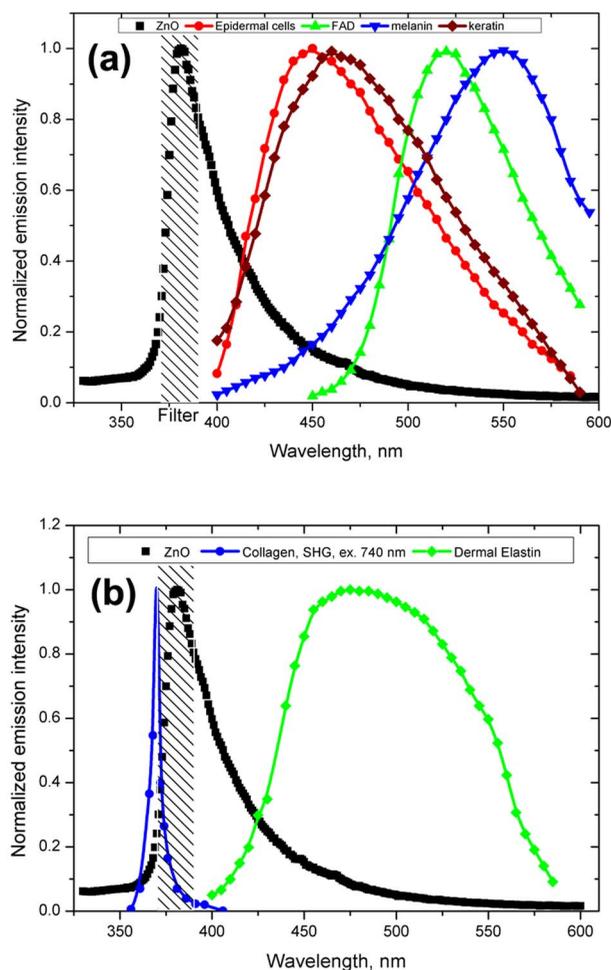

Fig. 1 Emission spectrum of ZnO-nano at an excitation wavelength of 320 nm (scatter plot, squares) superimposed on TPEF spectra of (a) epidermal cells (circles), similar to a spectrum of NAD[P]H; FAD (triangles); melanin (inverted triangles); keratin (diamonds), adapted from Ref. 14; and (b) elastin (diamonds), similar to collagen, adapted from Ref. 14; and the second-harmonic generation (SHG) spectrum of collagen calculated at a 740-nm fundamental wavelength. A dashed area designates FWHM of the bandpass filter BP380 used to discriminate ZnO PL signal against the skin autofluorescence.

range, and the water transparency window; and, second, to the reduced scattering efficiency of skin tissue at longer wavelengths.

In this paper, we communicate our results on application of multiphoton microscopy to study of ZnO nanoparticles penetration in human skin *in vitro* and *in vivo*. This is the first time, to the best of our knowledge, that the *in vivo* observation of inorganic PL nanoparticles in the morphology context of live cells and tissue has been reported. This will enable imaging of a new class of engineered nanostructures as applied to transdermal delivery and toxicology.

2 Materials and Methods

2.1 *Materials*

Dr. Lewinns' private formula (19% w/w) (Advanced Nanotechnology Ltd., WA, Australia) is comprised of 26 to 30-nm

mean size ZnO particles with preservatives of phenoxyethanol (0.3% w/w) and hydroxybenzoates (0.3% w/w) suspended in caprylic capric triglycerides.[17] These nanoparticles were fabricated by using the mechanochemical processing technology based on dry milling that induced chemical reactions through ball-powder collisions resulting in nanoparticle formation within a salt matrix. Particle size was determined by the chemistry of the reactant mixture, milling and heat treatment conditions.

For *in vivo* experiments, an area of 50 cm^2 of skin was selected on the forearm, cheek, shoulder, or feet of the subject and cleaned with ethanol. Four subjects of different ethnic background participated in this experiment: two Caucasian males, one Indian male, and a Chinese female aged 30 to 40, 40 to 50, and 25 to 30 yr, respectively.

For *in vitro* study, excised abdominal or breast human skin was obtained after plastic surgery.

2.2 Sample Treatment

Approximately 0.3 g of commercial Dr Lewinns' sun-blocking special formulation was applied evenly to the selected area of the human subjects and rubbed in for 5 min. The small amount was chosen arbitrarily to represent normal user application conditions. The area of application was small in comparison with the normal application of sunscreens for sun-blocking purposes. Subsequently, the treated area was noninvasively imaged using the multiphoton imaging system. A drop of water was applied to the region of skin being studied, followed by a 170-μm-thick microscope glass cover slip to ensure aberration-free imaging, and finally immersion oil between the coverslip and objective lens.

Images were acquired in three sessions: (1) immediately, (2) after 4 h, and (3) 24 h after the topical application, following washing. After session 1, the subject was allowed to move, as per usual daily routine. Session 3 was carried out following a shower at night, where the sun-blocking cream residue was washed away from the superficial layers of the skin. The rationale behind the times at which the images were carried out are as follows. Imaging immediately after application served as a control for time-lapse imaging. Imaging after 4 h was chosen as a representation of outdoors activities of the native population of southeast Queensland. The 24-h imaging was performed to verify whether prolonged exposure to sunscreens had any bearing on the ZnO penetration.

All experiments conducted on human subjects were done with approval of Princess Alexandra Hospital Research Committee (Approval No. 097/090, administered by the University of Queensland Human Ethics Committee). Each subject gave written consent.

2.3 Scanning Electron Microscope and Energy-Dispersive X-Ray Microanalysis

We employed a Philips XL30 FEG scanning electron microscope (SEM), with a backscattered electron detector and an integrated energy-dispersive x-ray (EDX) microanalysis system. The following procedure was used for sample preparation for SEM/EDX imaging and microanalysis. The ZnO nanoparticle formulation was applied to the excised skin sample, and incubated for 2 to 24 h. Several skin patches were tape-stripped 10 to 20 times on the areas of interest, while the other patches remained untouched. These nanoparticle-treated skin samples were fixed in 2.5% glutaraldehyde solution, a requirement of the SEM facilities used and workplace health and safety protocols, prior to freeze drying. Before imaging, all the samples were vacuum-coated with a 20- to 50-nm carbon coating. Conductive paint was applied to the aluminium stub holder. The SEM was operated at a 15- to 20-kV acceleration voltage and high vacuum, demanding all organic tissue to be fixed and dried. Images were obtained at a 11.3-mm working distance (the distance between lens and the sample stage). The numerical aperture (NA) was 6, and coarse was 7 units in the standard microscope settings. Focus, brightness, and contrast were adjusted for each image.

The fixed skin was cut into small cubical shape blocks approximately 1 cm^3 and snap-frozen with a specially made copper press that had been dipped in liquid nitrogen for 5 min. The samples were further dipped while in the press in liquid nitrogen and then freeze-dried. The small freeze-dried skin samples were mounted on the SEM, and imaged immediately.

2.4 Multiphoton Imaging

In the multiphoton microscopy (MPM) imaging system (JenLab GmbH Schillerstraße 107745 Jena Germany), ultrashort-pulse excitation laser light was tightly focused onto a sample by using a high-NA oil-immersion microscope objective (40 $\times$, NA1.3). This resulted in an enormous instantaneous intensity in the femtoliter focal volume that elicited the material's nonlinear optical response. Two-photon excited fluorescence (TPEF) is one manifestation of this nonlinear process. The fluorescence emission is localized exclusively within the focal volume resulting in the inherent "optical sectioning" property of multiphoton microscopy.[18] The thickness of each optical section was determined by the axial transfer function of the optical multiphoton imaging system, which was measured to be 2 μm for our experimental configuration. The excitation light represented a pulsed femtosecond laser, which was a tunable, computer-controlled titanium-sapphire laser (MaiTai, Spectra Physics) whose wavelength was set to 740 nm. The laser pulsewidth and repetition rate was 85 fs and 80 MHz, respectively. The incident optical power was set to 20 and 30 mW in stratum corneum and epidermis, respectively. A focused laser spot was raster-scanned across the sample using two galvanometer mirrors. The excited fluorescence was collected by the same objective lens. A dichroic mirror transmitted fluorescence to the detection photomultiplier tube (PMT), while reflecting the IR laser excitation light. In the detection arm, the fluorescence was split between two channels terminated by two optical detectors (PMTs) following preselected spectral filters. A narrow-bandpass interference filter (BP380, Omega Optical) centered at 380 nm, with a FWHM of 20 nm, was inserted in channel 1 to selectively detect ZnO PL signal. In channel 2, a broad bandpass filter (BG39, Schott glass color filter) with a long-wavelength cutoff of 700 nm was employed to block the excitation laser light so that the skin autofluorescence emission was captured. An image was formed by recording detector signals versus the focal spot position in the sample. The two images from the two channels were overlaid at a postprocessing stage.
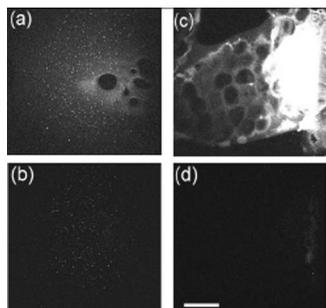
Fig. 2 MPM images: (a) and (b) ZnO-nano (scattered bright dots) the capric/caprilic oil film cast on a glass slide; (c) and (d) excised skin patch. Epidermal cellular architecture is clearly observable in (c). Images (a) and (c) and (b) and (d) are detected using the broadband (channel 1) and narrowband (channel 2) spectral filters, respectively. Scale bar 50 μm.

To optimize the spectral filter configuration in the detection arms, a preliminary imaging experiment using two samples was conducted. Sample 1 represented Dr Lewinns' cosmetic formulation diluted to a concentration of 0.005% and spin-coated on a glass slide to form nanoparticles and clusters. Sample 2 was a skin patch prepared, as already described in this section. The results of multiphoton imaging of these samples are presented in Fig. 2. Panels on the left- and right-hand-side columns show images of samples 1 and 2, respectively. The top and bottom images were obtained using the broadband (BG39) and UV narrowband (BP380) filters, respectively. Suppression of autofluorescence from caprylic/capric triglycerides solvent, visible as structured layout [Fig. 2(a)], is evident by comparing panels in Figs. 2(a) and 2(b). Likewise, the strong skin autofluorescence [Fig. 2(c)] is efficiently filtered by the UV narrowband filter [Fig. 2(d)]. The excised skin sample was deprived of NAD[P]H resulting in reduced autofluorescence intensity, probably dominated by FAD fluorescence.[14] Note that although the broadband emis-

sion in the visible spectrum of ZnO and ZnO-nano has been reported previously,[19] it was not observed in this study, probably owing to the high crystal quality of our ZnO-nano sample.

3 Results

Figure 3 shows our first *in vivo* images of human skin treated with the zinc oxide commercial formulation. Overlaid multiphoton images of human skin *in vivo* and ZnO-nano distribution, 4 hours after its topical application, are colorcoded green and red, respectively. *En face* optical sections of the skin are displayed from top left to bottom right at depths 0, 3, 14, 22, 30, and 48 μm from the skin surface designated S. The depth readout was corrected for the confocal parameter, calculated as $d_z = (z - z_0)n$, where $(z - z_0)$ denotes a difference between the axial position readout at a depth and top surface settings, and n denotes the mean refractive index of tissue, which was set to a mean value of 1.4 (Ref. 20). ZnO-nano patterns are clearly observable on the skin autofluorescence background, and especially pronounced on the topmost layers of the skin. Fine morphological details of unstained skin are clearly observable, e.g., cell structure in stratum granulosum (Fig. 3, bottom left panel), with dark nuclei and a granulated pattern in the cell cytoplasm, presumably, originated from NAD[P]H accumulated in mitochondria. As Fig. 3 shows, ZnO-nano predominantly remained on the topmost layer of SC within a several-micrometer layer (image panels S to 3 μm). The nanoparticle localization in the skin folds and dermatoglyph is clearly evident from Fig. 3 (14 μm to 30 μm). No penetration of ZnO-nano into the cells or extracellular space was observed.

Figure 4 shows images for the skin subdermal absorption of ZnO-nano after occupational exposure to the sunscreen formulation for various times. The skin of the three human subjects of different ethnical origins was imaged and analyzed using time-lapse *in vivo* MPM imaging of skin: shortly, 4 h
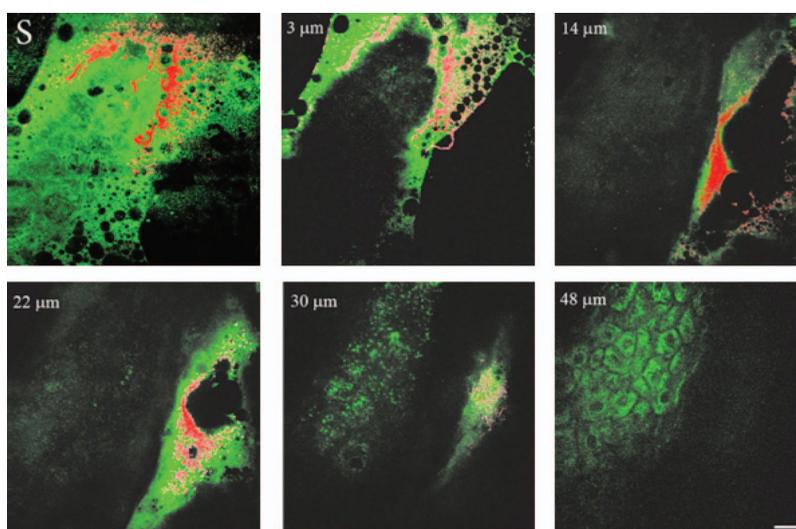

Fig. 3 Overlaid MPM images of human skin *in vivo* (color-coded green) and ZnO-nano distribution (color-coded red) 4 h after its topical application. *En face* optical sections of the skin are displayed from top left to bottom right at depths of 0, 3, 14, 22, 30, and 48 μm from the skin surface designed S and 3, 14, 22, 30, and 48 μm, respectively. Note ZnO localization in stratum corneum and in skin folds. No presence of nanoparticles in the stratum granulosum layer (ellipsoidal cells with dark nuclei) is observable. Scale bar 20 μm.
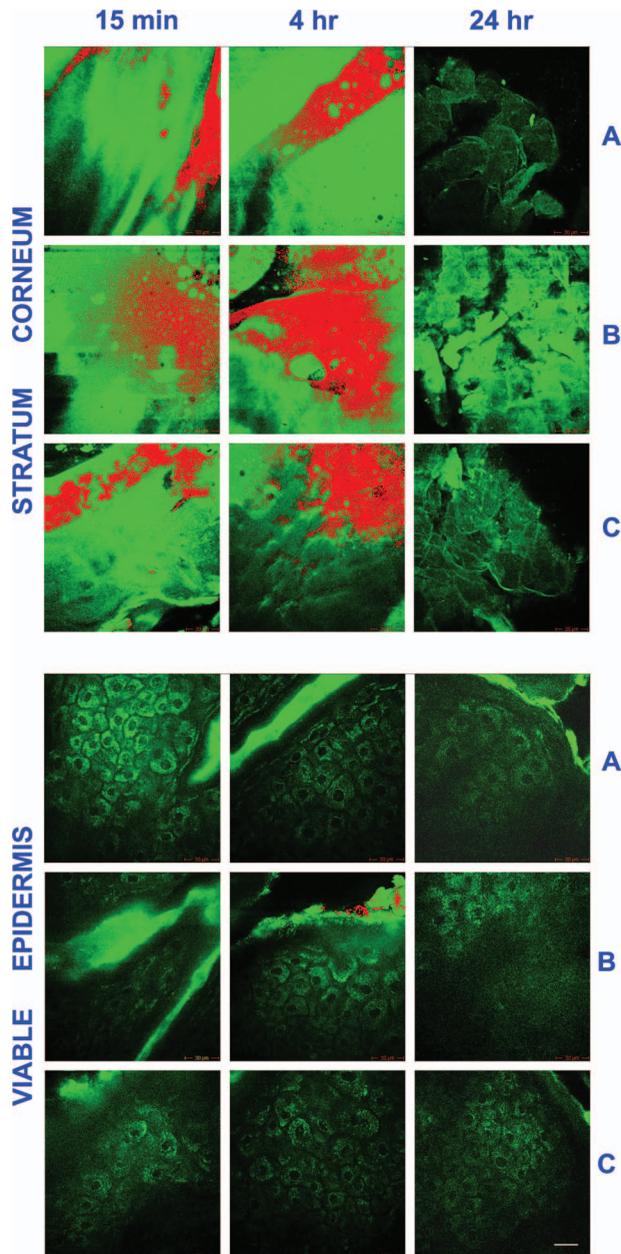
Fig. 4 Overlaid *in vivo* MPM images of ZnO-nano (color-coded red) distribution in human skin, forearm, dorsal side (color-coded green). Optical sections of stratum corneum and viable epidermis are grouped in two blocks. Each row displays images of three human subjects: Asian female, Chinese, aged below 30; Caucasian male, aged 30 to 40; and Indian male, aged 40 to 50, are designated by A, B, and C, respectively. Each column displays time-lapse image sequence acquired: 15 min, 4 h, 24 h, following the ZnO-formulation topical application. Scale bar 20 μm.

and 24 h after topical application of the formulation. No traces of ZnO were present in the viable epidermis (Viable Epidermis, Fig. 4), other than a well-confined island of ZnO in a skin fold (dark clearly outlined area) at 4 h after the sunscreen application in Caucasian skin, subject B. Images of SC acquired 24 h after sunscreen application show complete removal of sunscreen from skin, probably as a result of the daily shower routine exercised by each human subject in this
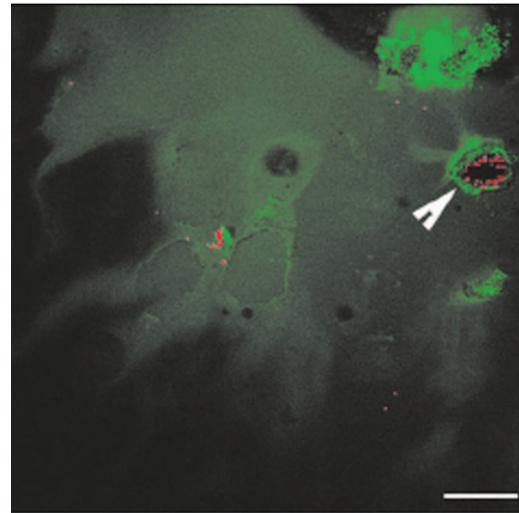

Fig. 5 Overlaid MPM images of the freshly (2 h) excised human skin (color-coded green) and ZnO-nano distribution (color-coded red) 4 hours after its topical application. An arrow points to the hair follicle canal, where a hair follicle shaft is not visible. ZnO formulation is localized around the hair follicle. Scale bar 20 μm.

experiment. In effect, this suggests ZnO-nano subdermal absorption after longer exposures is also unlikely.

MPM also enabled the investigation of alternative pathways of nanoparticle penetration, such as the appendages, as represented by the hair follicle canal. Since the hair follicle shaft can extend at a considerable depth in skin, 50 μm or greater, it can potentially represent an entry port of materials directly into the viable epidermis. Figure 5 shows an MPM cross-sectional image of the freshly (2 h) excised human skin topically treated with the sunscreen formulation. As described previously, no penetration of ZnO-nano is observable. At the same time, a prominent ZnO signal is noticeable at the perimeter of the hair follicle (white arrow). The hair shaft is not visible in the image. The sunscreen is localized in the hair follicle shaft without spreading to the neighboring cells and tissue. Our systematic studies of the nanoparticles penetration via this route confirmed this observation.[21]

To verify our MPM observations, we carried out high-resolution, high-sensitivity SEM/EDX measurements of ZnO nanoparticle penetration in the excised skin topically treated with ZnO-nano. Figure 6 shows the results of our observations. An SEM image shows a low-magnification morphological layout of the skin cross-section. In the central part of the image, a wedge-like skin fold converges inward. Several fragments of the bright-contrast debris are clearly localized in this skin fold. The EDX technique enables atomic species analysis locally. Integral x-ray spectra sampled at two sites of interest, SC/skin fold (solid circle) and epidermis (dashed circle) are shown in left-hand side panels Fig. 6. At least two prominent peaks of zinc (ZnK, ZnL, corresponding to excitation of the core electron shells in a zinc atom) and one oxygen peak were observed in the skin fold, as shown in panel EDX: stratum corneum. These are suggestive of the presence of ZnO in the skin fold, as expected considering the topical application of the sunscreen formulation on the skin. We note that ZnO-nano existed predominantly in an agglomerated phase. In contrast,
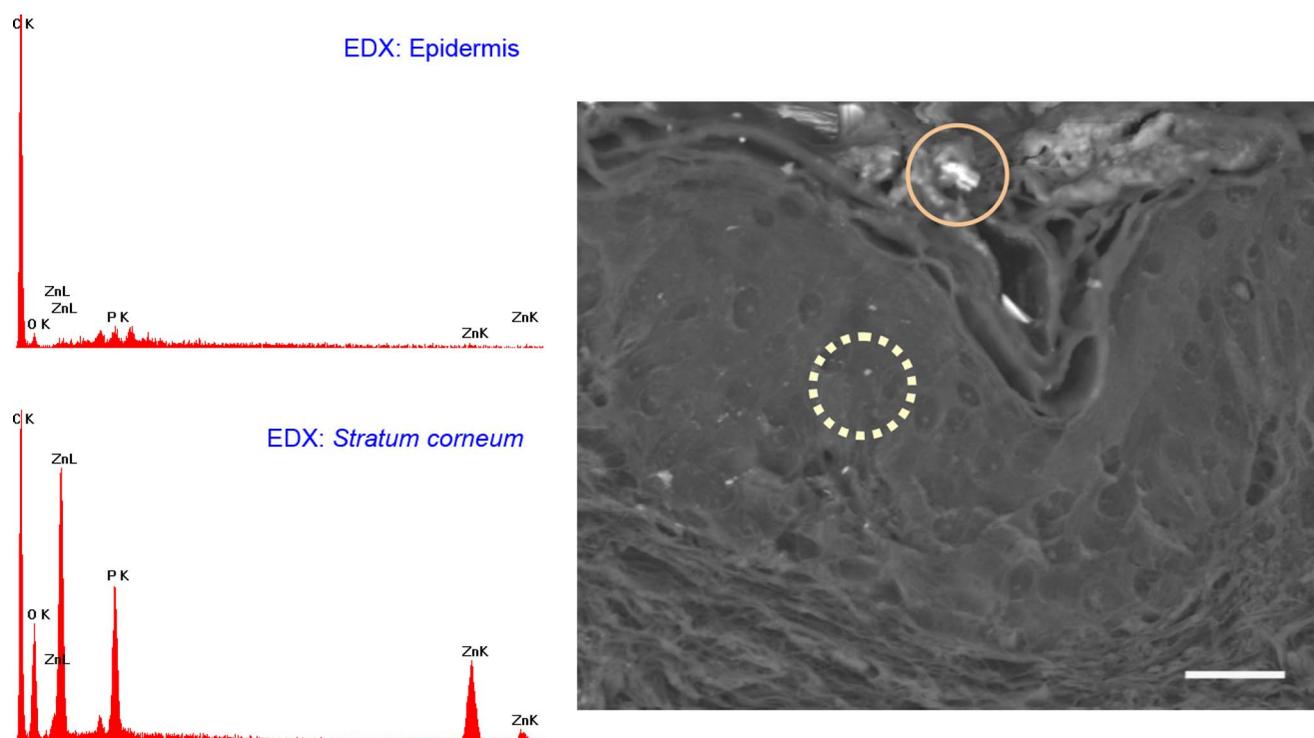
Fig. 6 SEM image (right-hand side panel) and EDX spectra (left-hand side panels) of the excised human skin topically treated with ZnO-nano. The EDX spectra sampled from the stratum corneum/skin fold (solid circle) and epidermis (dashed circle) areas are displayed in top (EDX: SC) and bottom (EDX: epidermis) left-hand side panels, respectively. Note EDX spectrum in SC shows two prominent peaks of atomic zinc origin (ZnL, ZnK). C, O, Zn, P, denote corresponding chemical elements. The ending letters K and L denote the characteristic binding energies of the core electron shells. Scale bar 20 μm.

no noticeable peaks were observed in the epidermis, as EDX-:epidermis panel shows. This result confirms our observation made by using multiphoton microscopy: ZnO-nano remained on the skin surface.

4 Discussion

The ZnO-nano nonlinear optical contrast on the cell autofluorescence background is remarkable and unexpected. This contrast could be due to several factors. First, the PL of ZnO nanoparticles is considerably enhanced compared to bulk ZnO. Guo et al.[22] have reported that the third-order nonlinear susceptibility $\chi^{(3)}_{ZnO}$ of ZnO-nano sized $d=4$ nm is almost 500-fold of that of bulk ZnO. As this enhancement is likely to be due to quantum confinement effects, ZnO-nano, with a size of several tens of nanometers, exhibits quantum dot properties. The systematic study of $\chi^{(3)}_{ZnO}$ versus ZnO-nano size in the size range of 6 to 18 nm has revealed a $\chi^{(3)}_{ZnO}$ quadratic size dependence, with $\chi^{(3)}_{ZnO}$ measured[23] to be 9.0×10^{-10} esu (expressed in cgs system of units) at $d=18$ nm and $\lambda=532$ nm. Second, ZnO-nano emission typically occurs in three major spectral bands centered at 385 nm (UV), 530 nm (green), and 590 nm (orange). The orange emission is broadband, and is due to oxygen interstitial defects, which disappear after high-temperature annealing in air.[19] Although the origin of the green broadband emission is not well understood, it is commonly believed to originate from oxygen vacancy defects. These defects may be situated on the surface of a ZnO-nano,

and hence amenable to surface treatment by capping with polymer.[22] Further, as the surface capping resulted in considerable suppression of the broadband emission in green (accompanied by the UV emission enhancement) several other capping-free ZnO-nano synthetic routes yield similar results.[19,24] Our sample exhibited no detectable emission bands in the visible spectral range (see Fig. 1). As maintained in the literature, the narrowband UV emission at 385 nm is unlikely to be due to direct bandgap transition, as the Stokes shift between the absorption and emission bands is too large. It is hypothesized and corroborated experimentally that the UV emission is due to deep donors associated with oxygen vacancies. A PL-induced electron populates this vacancy followed immediately by its recombination with an available hole (exciton recombination) accompanied by a UV photon emission. These donors are localized and their population density in the nanocrystal is high, leading to dramatic enhancement of the quantum confinement effect and enhanced UV emission.

To evaluate attainable contrast of ZnO-nano on the autofluorescence background of skin, we compared the two-photon excitation fluorescence signal from ZnO-nano with that of the endogenous fluorophores typical to skin. The two-photon absorption cross-section of ZnO-nano, $\sigma^{(2ph)}_{ZnO}$, which is governed by a third-order nonlinear process,[25] can be found by using the third-order nonlinear susceptibility, $\chi^{(3)}_{ZnO}$ of ZnO reported in the literature[26]

$$\sigma_{ZnO}^{(2ph)} = \frac{2\hbar\omega^2}{3Nn_0^2c^2\varepsilon_0} \, \mathrm{Im}\, \chi_{ZnO}^{(3)}, \qquad (1)$$

where $\hbar$ stands for the Plank's constant, $\omega = 2\pi c/\lambda$ is the optical angular frequency; N denotes nanoparticle concentration recalculated from the molar concentration of 10^{-4} M (reported in Ref. [22]); n_0 is the refractive index of ZnO at $\lambda = 532$ nm, which amounts to 2.0; c is speed of light; $\varepsilon_0 = 8.854 \times 10^{-12}$ F/m is the dielectric permeability constant. We convert $\chi_{ZnO}^{(3)}$ from 9.0×10^{-9} esu in the cgs system of units to $\chi_{ZnO}^{(3)} \cong 1.3 \times 10^{-17}$ m^2/V^2 in the SI system of units. Substitution of these values to Eq. (1) yields

$$\sigma_{ZnO}^{(2ph)} \cong 1.2 \times 10^{-49} \text{ m}^4 \text{ s/photon particle} \equiv 12 \text{ GM}, \quad (2)$$

for an 18-nm ZnO particle at $\lambda = 532$ nm, where we used a convention of 1 GM $\equiv 10^{-50}$ m^4 s/photon molecule for two-photon absorption cross-section. To evaluate a fluorescent signal from our sample, it is important to determine the nanoparticle action cross-section $\sigma_{ZnO}^{(TPEF)}$, which is defined as a product of the absorption cross-section and quantum yield Φ. Here Φ represents a number of fluorescence photons emitted per one absorbed photon (per two photons in TPEF). According to the literature reports,[27] the ZnO quantum yield varies depending on the crystal and surface quality, with a typical value of $\Phi = 0.02$. The two-photon action cross-section is evaluated to be $\sigma_{ZnO}^{(TPEF)} = 0.26$ GM for an 18-nm particle typical for our experimental conditions. This value is much less compared to that of water-soluble Qdots, $\sim 5 \times 10^4$ GM (Ref. [10]), and exogenous (externally introduced) fluorophores, such as fluorescein, ~ 50 GM. At the same time, $\sigma_{ZnO}^{(TPEF)}$ is favorably comparable to that of the dominant skin endogenous fluorophores, including reduced NAD[P]H, FAD, and retinol, whose $\sigma_{fluo}^{(TPEF)}$ does not exceed[28] 0.1 GM at 700 nm.

In the context of multiphoton imaging, the visibility of ZnO-nano material against the skin autofluorescence background is determined by its TPEF cross-section relative to that of endogenous fluorophores, its relative concentration, and its fluorescence emission spectral overlap with the dominant skin fluorophores. Skin autofluorescence has been investigated,[29] both in vitro and in vivo. The skin autofluorescence spectrum has been reported in the literature to feature three major component bands centered at 450, 520, and 625 nm on excitation in the wavelength range of 340 to 380 nm. The first two spectral bands corresponded to 75 and 25% of the total spectrum intensity, respectively.[15] These two peaks in the skin autofluorescence spectrum correspond to the fluorescence emission peaks of the endogenous skin fluorophores that include collagen, elastin, NAD[P]H, and FAD (Ref. [29]), whereas the peak at 625 nm corresponds to porphyrins. Skin autofluorescence background, excited as a result of the nonlinear optical processes, is somewhat different. It is spectrally separated into an intense SHG signal from collagen, which occurs at a precisely half the laser excitation wavelength (UV range), a narrow emission band from 400 to 430 nm, and a broadband emission from 430 to 600 nm (see Fig. 1) (Ref. [14]). In live skin, the autofluorescence spectrum in epidermis is dominated by NAD[P]H, as this coenzyme is involved in cellular energy metabolism. Vitamin derivatives, such as flavins, also have a noticeable contribution to the autofluores-

cence spectrum of epidermis in vivo. In the excised epidermis, the NAD[P]H contribution is markedly reduced due to degradation of the metabolic cycles, resulting in the reduced autofluorescence level and its spectral red-shift due to keratin and to some extent flavin components.

Note that the ZnO UV absorption band is advantageous to enable spectral discrimination of its emission signal from most endogenous fluorophores of skin, including NAD[P]H, riboflavin, folic acid, and retinol, all having emission bands in visible. At the same time, the emission band of pyridoxine falls[28] into that of ZnO, and demands attention in certain imaging scenarios. However, for the nanoparticle transdermal penetration study, confined to the SC and viable epidermis, such collagen-related molecules as pyridoxine, pose little problem, since they are predominantly present in dermis. The SHG signal from collagen [see Fig. 1(b)] did not present a problem due to its predominant location in the dermis. Further, this signal wavelength is precisely half the wavelength of the excitation source so that it may fall outside the ZnO PL spectral range. The ZnO-nano UV PL spectral band may overlap with that of the other endogenous fluorophores, leading to a degraded imaging contrast.

The femtosecond laser excitation wavelength of 740 nm used in our experiments is suboptimal for the excitation of ZnO TPEF, as the ZnO bandgap width of 3.4 eV ($\lambda = 350$ nm) requires two-photon excitation at a fundamental wavelength of 700 nm. At the same time, $\sigma_{ZnO}^{(2ph)}$ dependence versus λ falls off gradually from 350 to 380 nm, whereas $\sigma_{ZnO}^{(2ph)}$ ($\lambda = 740$ nm) $\cong 0.4\sigma_{ZnO}^{(2ph)}$ ($\lambda = 700$ nm) (Ref. [23]). At the same time, Iripman et al. have noted a steep increase of $\mathrm{Im}\, \chi_{ZnO}^{(3)}$ versus the laser intensity.[23] Therefore, our evaluation of $\sigma_{ZnO}^{(2ph)}$ [see Eq. (2)] must be treated as only a rough estimation. Note that, unlike in case of free excitons, characterized by $\sigma^{(2ph)} \propto d^3$, $\sigma_{ZnO}^{(2ph)} \propto d^2$ in the size range $d = 6$ to 18 nm, revealing the bound exciton nature of ZnO-nano. Also $\sigma_{ZnO}^{(2ph)}$ is sensitive to the crystal/surface quality. Our preliminary data on the nonlinear optical signal intensity versus input power suggests that three-photon nonlinear optical absorption makes a slight additional contribution to the excitation of ZnO-nano.[16] Although $\mathrm{Im}\, \chi_{ZnO}^{(3)}$ has been recently measured, no data on the three-photon absorption cross-section of ZnO-nano has been reported to the best of our knowledge.

Application of the adapted multiphoton imaging system to imaging ZnO-nano enabled us to examine the existing hypothesis on the nanoparticle penetrability through the normal intact skin. Importantly, we have been able to investigate this question in vivo and show that the ZnO-nano did not penetrate human skin either in vitro or in vivo. This work is important, as it addresses the first aspect that may have caused ZnO-nano toxicity penetration. This work suggests that ZnO-nano, of about 15 to 30 nm in size, does not penetrate human skin. In contrast, the smaller molecules, such as salicylic acid (0.5 nm), do penetrate the skin.[30] This is consistent with a number of in vitro investigations of cosmetic-origin ZnO-nano penetration in skin that have been reported.[31,32] In our study, we used caprylic capric triglycerides formulation for ZnO-nano, which promotes passive diffusion of nanoparticles via a lipophilic intercellular pathway. This pathway represents the principle transdermal penetration route, and hence repre-

sents the most stringent test of the ZnO-nano penetrability, except for active skin enhancers. Electron micrographs of human skin show ZnO-nano mineral components are present on the surface of the skin and around desquaming corneocytes[17] and not in deeper tissues. Australia's Therapeutic Goods Agency has actively supported the notion that ZnO and TiO_2 remain on the surface of the skin and in the outer dead layer (SC) of the skin.[26]

The data contrasts the most recent results by Ryman-Rasmussen et al. that Qdots of the size range of 15 to 40 nm did penetrate porcine skin, long considered a reliable model of the human skin.[33] Three types of the Qdot nanoparticles with positive, neutral, and negative charges on the Qdot surface were found in epidermis and dermis passed the SC, followed the skin topical application *in vitro*. These Qdots were shown to cause a severe immunological cellular response, ultimately resulting in cell apoptosis.[34] The size range of our ZnO nanoparticles (15 to 30 nm) was commensurable with that reported by the authors. Based on our results[21] (also, to be communicated elsewhere), we argue that porcine skin represents a poor model of human skin in the context of transdermal penetrability to nanoparticles. Receptor phase penetration of zinc through the human epidermal membrane has been observed over 24 h using the Franz cell-based technique,[17] although it was likely to be negligible and in a form of hydrolyzed zinc ions rather than integral ZnO-nano.

In this context, it is unlikely that ZnO-nano would be toxic if skin penetration had occurred. Cytotoxicity, genotoxicity, and photogenotoxicity studies on TiO_2 or other insoluble nanoparticles should be interpreted with caution, since such toxicities may be secondary to phagocytosis of mammalian cells exposed to high concentrations of insoluble particles. Studies on wear debris particles from surgical implants and other toxicity studies on insoluble particles support the traditional toxicology view that the hazard of small particles is mainly defined by the intrinsic toxicity of particles, as distinct from their particle size. There is little evidence supporting the principle that smaller particles have greater effects on the skin or other tissues or produce novel toxicities relative to micro-sized materials. Overall, the current weight of evidence suggests that nano-materials such as nano-sized vesicles or ZnO and TiO_2 nanoparticles currently used in cosmetic preparations or sunscreens pose no risk to human skin or human health, although other nanoparticles may have properties that warrant safety evaluation on a case-by-case basis before human use.

5 Conclusion

We investigated *in vitro* and *in vivo* skin penetrability to nanoparticles of the size range typical to that used in cosmetic products, i.e., 15 to 30 nm. For the first time, the application of multiphoton microscopy has enabled imaging of both the wide bandgap nanostructures, e.g., ZnO-nano, and skin tissue/cellular architecture. ZnO appeared to have surprisingly high visibility against the skin autofluorescence background, which was attributed to its enhanced nonlinear two-photon action cross-section $[\sigma_{ZnO}^{(2ph)} \sim 0.26 \text{ GM}]$ favorably compared to that of the skin endogenous fluorophores, e.g., NAD[P]H and FAD; and "transparency window" of skin autofluorescence at 380 ± 20 nm occupied by the ZnO-nano principle photolumi-

nescence. Nanoparticles have been found to stay on the SC, or fell into skin folds or hair follicle roots, thus, confirming safety of the ZnO-nano-based cosmetic products *in vivo*.

References

1. G. J. Nohynek, J. Lademann, C. Ribaud, and M. S. Roberts, "Grey goo on the skin? Nanotechnology, cosmetic and sunscreen safety," *Crit. Rev. Toxicol.* **37**(3), 251–277 (2007).
2. G. P. H. Dietz and M. Bahr, "Delivery of bioactive molecules into the cell: the Trojan horse approach," *Mol. Cell. Neurosci.* **27**(2), 85–131 (2004).
3. A. Beduneau, P. Saulnier, and J. P. Benoit, "Active targeting of brain tumors using nanocarriers," *Biomaterials* **28**(33), 4947–4967 (2007).
4. Z. P. Xu, Q. H. Zeng, G. Q. Lu, and A. B. Yu, "Inorganic nanoparticles as carriers for efficient cellular delivery," *Chem. Eng. Sci.* **61**(3), 1027–1040 (2006).
5. P. H. Youl, P. D. Baade, M. Janda, C. B. Del Mar, D. C. Whiteman, and J. F. Aitken, "Diagnosing skin cancer in primary care: how do mainstream general practitioners compare with primary care skin cancer clinic doctors?" *Med. J. Aust.* **187**(4), 215–220 (2007).
6. R. Alvarez-Roman, A. Naik, Y. Kalia, R. H. Guy, and H. Fessi, "Skin penetration and distribution of polymeric nanoparticles," *J. Controlled Release* **99**(1), 53–62 (2004).
7. K. F. Lin, H. M. Cheng, H. C. Hsu, L. J. Lin, and W. F. Hsieh, "Band gap variation of size-controlled ZnO quantum dots synthesized by sol-gel method," *Chem. Phys. Lett.* **409**(4–6), 208–211 (2005).
8. R. Dunford, A. Salinaro, L. Z. Cai, N. Serpone, S. Horikoshi, H. Hidaka, and J. Knowland, "Chemical oxidation and DNA damage catalysed by inorganic sunscreen ingredients," *FEBS Lett.* **418**(1–2), 87–90 (1997).
9. H. A. Jeng and J. Swanson, "Toxicity of metal oxide nanoparticles in mammalian cells," *J. Environ. Sci. Health, Part A: Toxic/Hazard. Subst. Environ. Eng.* **41**(12), 2699–2711 (2006).
10. D. R. Larson, W. R. Zipfel, R. M. Williams, S. W. Clark, M. P. Bruchez, F. W. Wise, and W. W. Webb, "Water-soluble quantum dots for multiphoton fluorescence imaging in vivo," *Science* **300**(5624), 1434–1436 (2003).
11. H.-Y. Lee, Y.-R. Chang, K. Chen, C.-C. Chang, D.-S. Tsai, C.-C. Fu, T.-S. Lim, Y.-K. Tzeng, C.-Y. Fang, C.-C. Han, H.-C. Chang, and W. Fann, "Mass production and dynamic imaging of fluorescent nanodiamonds," *Nat. Nanotechnol.* **3**, 284–288 (2008).
12. Z. F. Li and E. Ruckenstein, "Water-soluble poly(acrylic acid) grafted luminescent silicon nanoparticles and their use as fluorescent biological staining labels," *Nano Lett.* **4**(8), 1463–1467 (2004).
13. H. M. Cheng, K. F. Lin, H. C. Hsu, and W. F. Hsieh, "Size dependence of photoluminescence and resonant Raman scattering from ZnO quantum dots," *Appl. Phys. Lett.* **88**(26), 261909 (2006).
14. J. A. Palero, H. S. de Bruijn, A. V. van den Heuvel, H. Sterenborg, and H. C. Gerritsen, "Spectrally resolved multiphoton imaging of in vivo and excised mouse skin tissues," *Biophys. J.* **93**(3), 992–1007 (2007).
15. R. H. Na, I. M. Stender, L. X. Ma, and H. C. Wulf, "Autofluorescence spectrum of skin: component bands and body site variations," *Skin Res. Technol.* **6**(3), 112–117 (2000).
16. D. C. Dai, S. J. Xu, S. L. Shi, M. H. Xie, and C. M. Che, "Efficient multiphoton-absorption-induced luminescence in single-crystalline ZnO at room temperature," *Opt. Lett.* **30**(24), 3377–3379 (2005).
17. S. E. Cross, B. Innes, M. S. Roberts, T. Tsuzuki, T. A. Robertson, and P. McCormick, "Human skin penetration of sunscreen nanoparticles: in-vitro assessment of a novel micronized zinc oxide formulation," *Skin Pharmacol. Appl. Skin Physiol.* **20**(3), 148–154 (2007).
18. K. Konig, A. Ehlers, F. Stracke, and I. Riemann, "In vivo drug screening in human skin using femtosecond laser multiphoton tomography," *Skin Pharmacol. Appl. Skin Physiol.* **19**(2), 78–88 (2006).
19. H. M. Cheng, H. C. Hsu, S. L. Chen, W. T. Wu, C. C. Kao, L. J. Lin, and W. F. Hsieh, "Efficient UV photoluminescence from monodispersed secondary ZnO colloidal spheres synthesized by sol-gel method," *J. Cryst. Growth* **277**(1–4), 192–199 (2005).
20. V. Tuchin, *Tissue Optics: Light Scattering Methods and Instruments for Medical Diagnosis*, Kluwer Academic Publishers, Boston (2000).
21. A. J. X. Zhao, J. A. Ross, M. Sarkar, W. Sanchez, A. V. Zvyagin, and M. S. Roberts, "Nanoparticles penetration through human skin, much ado about nothing?", presented at the Trailblazing the Skin Frontier: Evidence Base, Opportunities&Training, George Washington Univer-

sity, Washington, DC, 11–13 August 2007 (2007), pp. 22.

22. L. Guo, S. H. Yang, C. L. Yang, P. Yu, J. N. Wang, W. K. Ge, and G. K. L. Wong, "Highly monodisperse polymer-capped ZnO nanoparticles: preparation and optical properties," *Appl. Phys. Lett.* **76**(20), 2901–2903 (2000).

23. L. Irimpan, V. P. N. Nampoori, P. Radhakrishnan, B. Krishnan, and A. Deepthy, "Size-dependent enhancement of nonlinear optical properties in nanocolloids of ZnO," *J. Appl. Phys.* **103**(3), 033105 (2008).

24. M. M. Demir, R. Munoz-Espi, I. Lieberwirth, and G. Wagner, "Precipitation of monodisperse ZnO nanocrystals via acid-catalyzed esterification of zinc acetate," *J. Mater. Chem.* **16**(28), 2940–2947 (2006).

25. R. L. Sutherland, *Handbook of Nonlinear Optics*, Marcel Dekker, New York (1996).

26. "A review of the scientific literature on the safety of nanoparticulate titanium dioxide or zinc oxide in sunscreens", edited by A. Therapeutic Goods Administration (Australian Government, Department of Health and Aging, 2006).

27. M. Schubnell, I. Kamber, and P. Beaud, "Photochemistry at high temperatures—potential of ZnO as a high temperature photocatalyst," *Appl. Phys. A: Mater. Sci. Process.* **64**(1), 109–113 (1997).

28. W. R. Zipfel, R. M. Williams, R. Christie, A. Y. Nikitin, B. T. Hyman, and W. W. Webb, "Live tissue intrinsic emission microscopy using multiphoton-excited native fluorescence and second harmonic

generation," *Proc. Natl. Acad. Sci. U.S.A.* **100**(12), 7075–7080 (2003).

29. N. Kollias, R. Gillies, M. Moran, I. E. Kochevar, and R. R. Anderson, "Endogenous skin fluorescence includes bands that may serve as quantitative markers of aging and photoaging," *J. Invest. Dermatol.* **111**(5), 776–780 (1998).

30. K. Harada, T. Murakami, E. Kawasaki, Y. Higashi, S. Yamamoto, and N. Yata, "Invitro permeability to salicylic-acid of human, rodent, and shed snake skin," *J. Pharm. Pharmacol.* **45**(5), 414–418 (1993).

31. Z. S. Kertesz and A. Z. Kiss, "Quality of skin as a barrier to ultra-fine particles," Contribution of the IBA Group to the Nanoderm EU-5 Project (2003–2004).

32. C. G. J. Hayden, S. E. Cross, C. Anderson et al., "Sunscreen penetration of human skin and related keratinocyte toxicity after topical application," *Skin Pharmacol. Appl. Skin Physiol.* **18**(4), 170–174 (2005).

33. J. P. Ryman-Rasmussen, J. E. Riviere, and N. A. Monteiro-Riviere, "Penetration of intact skin by quantum dots with diverse physicochemical properties," *Toxicol. Sci.* **91**(1), 159–165 (2006).

34. J. P. Ryman-Rasmussen, J. E. Riviere, and N. A. Monteiro-Riviere, "Surface coatings determine cytotoxicity and irritation potential of quantum dot nanoparticles in epidermal keratinocytes," *J. Invest. Dermatol.* **127**(1), 143–153 (2007).